Rates of low-pH biological Fe(II) oxidation in the Appalachian Bituminous Coal Basin and the Iberian Pyrite Belt

CrossMark

Lance N. Larson [a,1,*], Javier Sánchez-España [b], William Burgos [a]

[a] Department of Civil and Environmental Engineering, The Pennsylvania State University, University Park, PA 16802, United States
[b] Instituto Geológico y Minero de España (IGME), Tres Cantos, Spain

ABSTRACT

Low-pH Fe(II) oxidation can be exploited for the treatment of acid mine drainage (AMD). However, natural or engineered terraced iron formations (TIFs) are underutilized for AMD treatment because of uncertainties with respect to treatment performance. To address this problem we measured the rates of Fe(II) oxidation multiple times at eight sites in the Appalachian Bituminous Coal Basin and at three sites in the Iberian Pyrite Belt (IPB). Longitudinal geochemical transects were measured downstream of emergent anoxic AMD sources. Water velocities were measured at each sampling location and used to transform concentration versus distance profiles into concentration versus travel time for kinetic analysis of field data. Zero-order Fe(II) oxidation rates ranged from 8.60 to 81.3×10^{-7} mol L^{-1} s^{-1} at the Appalachian sites and 13.1 to 67.9×10^{-7} mol L^{-1} s^{-1} at the IPB sites. First-order Fe(II) oxidation rate constants ranged from 0.035 to 0.399 min^{-1} at the Appalachian sites and 0.003 to 0.010 min^{-1} at the IPB sites. Faster rates of Fe(II) oxidation were measured at two sites (one in Appalachia and one in IPB) where the emergent pH values were the lowest and little to no oxidative precipitation of Fe(III) occurred. Laboratory-based rates of Fe(II) oxidation were measured with TIF sediments and emergent AMD collected from seven Appalachian sites. First-order laboratory rate constants normalized to sediment biomass concentrations (measured by phospholipid fatty acids; PLFA) were positively correlated to first-order field rate constants. Biomass composition was relatively similar between all sites, and predominantly comprised of proteobacteria and general PLFAs. A zero-order lab-based removal rate for dissolved Fe(T) was used to calculate area-based design criteria of 2.6–8.7 g Fe day^{-1} m^{-2} (GDM) for both natural and engineered TIFs.

© 2014 Elsevier Ltd. All rights reserved.

1. Introduction

Active and historical mining activities threaten ecosystems throughout the world. It is estimated that 95–99.999% of earth material from Cu, Pb, Zn, Au, and Ag mining operations becomes waste material (Nordstrom, 2011). Acid mine drainage (AMD) occurs when physical and chemical weathering of sulfides in mine ores facilitate proton releasing reactions (Kirby and Cravotta, 2005; Nordstrom et al., 1999). The ensuing pH drop enhances the solubility of metals such as iron (Fe), aluminum (Al), manganese (Mn), metalloids such as arsenic (As), and sulfate (SO_4^{2-}), resulting in hazardous or toxic concentrations transported into aquatic systems. Some of the most notorious mining-impacted environments are associated with metal mining, such as the Berkley Pit in

Montana (Gammons et al., 2010; Pellicori et al., 2005), Iron Mountain, California (Druschel et al., 2004; Edwards et al., 1999; Nordstrom et al., 1999), and Rio Tinto, Spain (Cánovas et al., 2008; Gammons et al., 2008; Sánchez España et al., 2007b). In the Appalachian region of the United States, AMD is the number one source of pollution to waterways (Pennsylvania Department of Environmental Protection (DEP), 2010). Although overall water quality in central Pennsylvania has improved since the 1970s, AMD pollution still impairs approximately 1930 km of streams (Trout Unlimited, 2011).

The oxidation of Fe(II) and the subsequent precipitation of Fe(III) are key reactions for AMD treatment. The kinetics of abiotic Fe(II) oxidation at circumneutral pH has been modeled according to (Stumm and Morgan, 1996):

$$\frac{d[Fe(II)]}{dt} = -k_{abiotic}[Fe(II)][O_2][H^+]^{-2} \quad (1)$$

where $k_{abiotic}$ is the Fe(II) oxidation rate constant (time^{-1}), [Fe(II)] is the concentration of dissolved ferrous iron (M), [O_2] is the concentration of dissolved oxygen (M), and [H^+] is the concentration of protons (M). Due to the exponent on the [H^+] term in Eq. (1), small

---

* Corresponding author. Address: Department of Civil and Environmental Engineering, The Pennsylvania State University, 212 Sackett Building, University Park, PA 16802, United States. Tel.: +1 202 513 6279.

E-mail address: llarson@nrdc.org (L.N. Larson).

[1] Current address: Natural Resources Defense Council, 1152 15th Street NW, Suite 300, Washington, DC 20005, United States.

changes in solution pH greatly influence the rate of Fe(II) oxidation (where rate increases sharply as pH increases). Below pH ∼5, the spontaneous abiotic Fe(II) oxidation rate is slow, although it can be influenced by a number of anions, organic ligands, and certain minerals (Cornell and Schwertmann, 1996). Under acidic conditions (pH <∼4), Fe(II) oxidation is catalyzed by acidophilic organisms (Hallberg, 2010) as Fe(II) becomes an energetically favorable electron donor for microorganisms (Hedrich et al., 2011). As acidophilic organisms oxidize Fe(II), Fe(III) will precipitate from solution as various minerals, typically schwertmannite [nominally $Fe_8O_8(OH)_6$ (SO_4)] or ferrihydrite (Bigham et al., 1996; Burgos et al., 2012; Sánchez España et al., 2007b; Yu et al., 1999). The precipitation of Fe(III)-minerals results in the development of terraced iron formations (TIFs) and the removal of dissolved total Fe(T) from solution (Brown et al., 2010; DeSa et al., 2010; Sánchez España et al., 2007a). For the applied purpose of using TIFs for AMD treatment, it remains unclear how site-specific geochemistry, hydrology, seasonal variability, and microbial diversity influence field-scale low-pH Fe(II) oxidation rates.

Rate expressions for biologically-catalyzed low-pH Fe(II) oxidation proposed in the literature are variable, ranging from multi-parameter, nth-order expressions (Kirby et al., 1999; Pesic et al., 1989) to pseudo first-order or zero-order expressions (Chen and Jiang, 2012; Sánchez España et al., 2007a). For ponds designed to collect low-pH Fe(II)-rich AMD, Kirby et al. (1999) modeled biological Fe(II) oxidation according to:

$$d[Fe(II)]/dt = -k_{bio}C_{bact}[Fe(II)][O_2][H^+] \qquad (2)$$

where k_{bio} is the biological rate constant ($L^3 mg^{-1} mol^{-2} s^{-1}$), C_{bact} is the concentration of iron-oxidizing bacteria ($mg L^{-1}$), and [ ] represents dissolved concentrations ($mol L^{-1}$). In contrast to abiotic Fe(II) oxidation, the rate of biological Fe(II) oxidation increases as pH decreases. At a site in Pennsylvania, rotating biological contactors (RBCs) were used to treat AMD and Fe(II) oxidation was observed to be first-order with respect to the influent Fe(II) concentration. Treatment efficiency increased with temperature and hydraulic residence time (Olem and Unz, 1977). Rates of Fe(II) oxidation measured in wetlands designed for AMD treatment were better fit using a first-order versus zero-order model (Tarutis et al., 1999). Rates of Fe(II) oxidation measured in the Iberian Pyrite Belt (IPB) have been reported to be zero-order (Sánchez España et al., 2007a). Sánchez España et al. (2007a) also measured zero-order rates of Fe(II) oxidation in corresponding laboratory experiments but found the field rates were almost an order of magnitude faster than the laboratory rates.

Detailed rate laws for biological Fe(II) oxidation have been developed from laboratory studies using pure cultures of Fe(II)-oxidizing bacteria. Pesic et al. (1989) constructed a model to describe Fe(II) oxidation rates by *Thiobacillus ferrooxidans* as a function of Fe(II), pH, dissolved oxygen, and cell concentration (Williamson et al., 2006). An energetics-based model for *T. ferrooxidans* growth was developed by accounting for carbon fixation rates through the Calvin-Benson cycle (Nagpal, 1997). Rates of Fe(II) oxidation by *Acidithiobacillus ferrooxidans* were enhanced when Fe(III) (hydr)oxide precipitation was inhibited, presumably due to Fe solids interfering with cell proton diffusion (Meruane and Vargas, 2003). It remains unclear how biotic Fe(II) oxidation models can be scaled to predict field performance.

The ability of TIFs to remove dissolved Fe via low-pH Fe(II) oxidation represents an attractive passive treatment technology as little to no external energy inputs are required. Design guidelines for TIF-based AMD treatment are currently nonexistent. Remediation design is limited because reported rates of low-pH Fe(II) oxidation are highly variable, often spanning three to four orders of magnitude at a fixed pH value (Kirby and Elder-Brady, 1998). The objectives of this research were to (1) measure and compare low-pH Fe(II) oxidation rates across a number of TIFs that vary with respect to mine source (i.e., metal vs coal), AMD chemistry, hydrological and physical conditions, and seasonal variability; (2) simulate field conditions using controlled, laboratory flow-through experiments, and; (3) determine how laboratory rates and field scale observations can be used to predict the performance of engineered TIFs.

2. Materials and methods

2.1. Site locations and descriptions

Eleven mine-impacted sites were sampled. Eight sites were located in the Appalachian Bituminous Coal Basin of the United States and three sites were located in the IPB of southwestern Spain (Fig. 1). These sites were selected due to diverse geochemical and hydrological conditions (Table 1), and to compare rates of Fe(II) oxidation in Appalachian coal mine drainage versus IPB metal mine drainage. Sites in the US contained discharges associated with bituminous coal or clay mining that occurred in the mid-to-late twentieth century. A representative site photo is presented in Supplemental-1. Sites in the US were sampled three to six times between September 2010 and May 2013. Sites in Spain were sampled twice in March and May 2012, months that historically span a decline in rainfall and base flow (Sánchez España et al., 2005; Supplemental-2).

The US sites were divided into natural and engineered TIFs, the former formed below artesian AMD springs with no human intervention and the latter were shallow channels integrated into passive treatment systems. The natural TIFs included Brubaker Run (BR), Scalp Level (SL), Sulphur Run (SR), Summerlee-Natural (SUM-N), and Upper Red Eyes (UR). The engineered sites included Dents Run (DR), Greens Run (GR), and Summerlee-Engineered (SUM-E). Sites in the IPB contained discharges associated with metal mining that occurred since pre-Roman times until present-day (Leistel et al., 1997). The former ore deposits were always composed of massive sulfides with dominant pyrite. The IPB sites were identified as Rio Tintillo (RTL), La Zarza–Perrunal (LZP), and Peña del Hierro (PDH).

2.2. Field sampling

For each site, geochemical profiles were established as longitudinal transects downstream from the emergent source using a combination of field measurements, collection of water and sediment samples, and physical site characteristics, along a single flow path which conveyed the majority of the water across each TIF. Portable field meters were used to measure pH, oxidation–reduction potential (ORP), dissolved oxygen (DO), and temperature (Beckman BKA57201 ATC; HACH40d LDO portable meters). The pH meter was calibrated using pH 1.68, 4.0, and 7.0 standards, while the ORP meter was calibrated with a freshly prepared +228 mV Zobel standard solution. We also used a multiparametric probe (Hydrolab MS5, Hach Company) to measure pH, ORP, DO, temperature and specific conductance at the IPB sites. Water samples were collected at each location, filtered (0.2 μm), chemically preserved (according to each analyte), transported on ice, and stored at 4 °C, until analysis (<7 d after collection). Rates of Fe(II) oxidation in the field were calculated using concentrations of dissolved Fe(II) versus travel time. Water velocities were measured at each sampling location and used to calculate travel times. Water velocities were measured using a food color dye as a tracer along with a stopwatch and tape measure. The rate of Fe(II) oxidation was modeled as first-order with respect to dissolved Fe(II) and
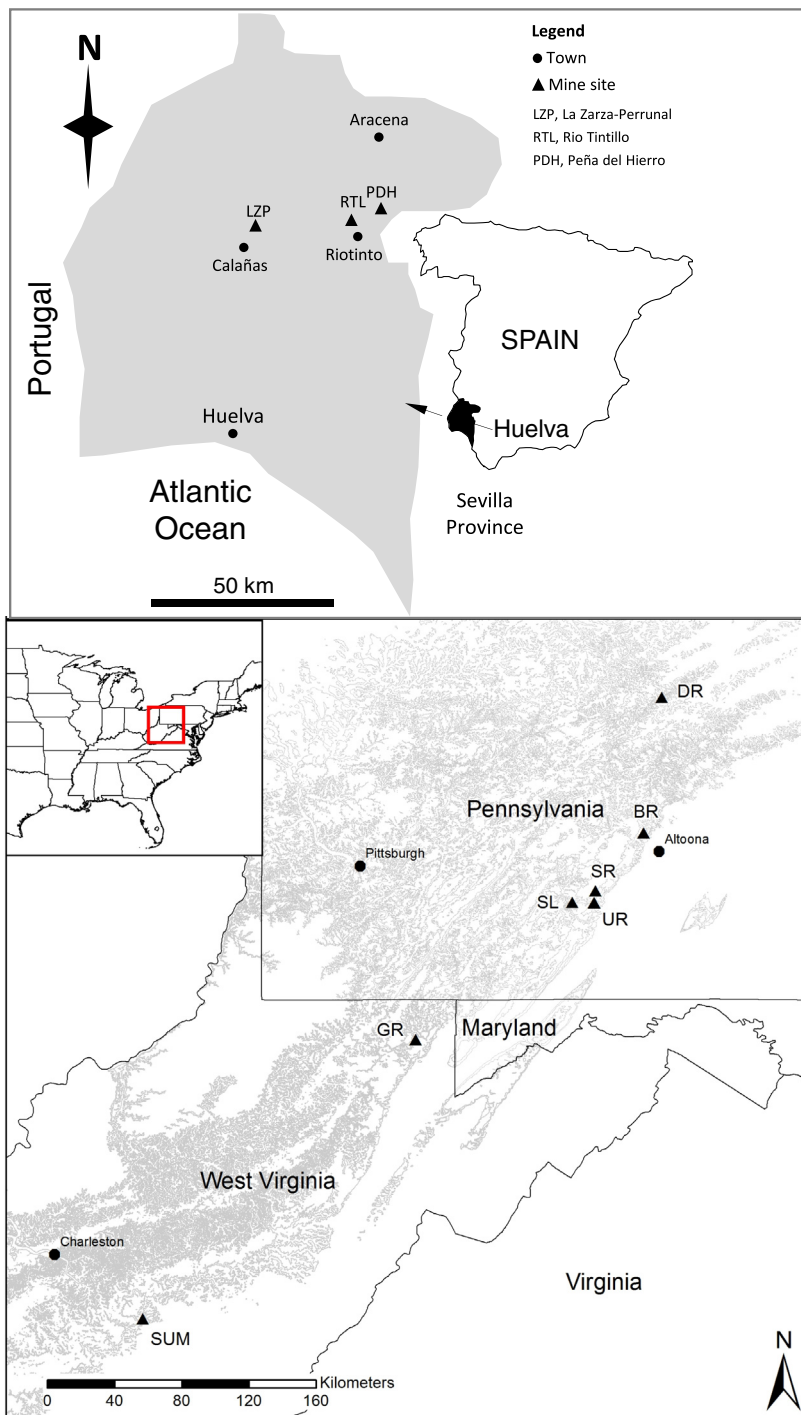
Fig. 1. Sampling locations for TIF sites in the Appalachian Bituminous Coal Basin in the US and the Iberian Pyrite Belt in Spain. Light gray zones show the location of coal fields in western Pennsylvania and West Virginia. SUM-E and SUM-N are located approximately 20 m apart and are collectively labeled as 'SUM'. Filled circles represent cities and filled squares represent field sites.

zero-order rates were calculated for comparisons to other studies (Table 2).

2.3. Laboratory experiments

Sediment pieces were cut from the TIFs and immediately placed into plastic containers similar to those used as the flow-through reactor vessels (13 cm × 8.2 cm × 6.4 cm; $l \times w \times d$). Sediment pieces were collected from the surface layer of the TIF, typically no thicker than 1 cm, and fashioned to similar shapes as the reactor vessel. Cemented sediments were extremely difficult to remove from the concrete channel at GR and shipping logistics precluded lab work with any of the Spanish sites. Water for flow-through reactors was collected from each AMD emergence into 38 L high density polyethylene (HDPE) plastic carboys and filled to eliminate or minimize headspace. Upon returning to the laboratory, the AMD was filtered (0.2 μm), flushed with $N_2(g)$ for 1 h, capped and sealed with parafilm, and stored at 4 °C for no more than one week.

Table 1

Geochemical characteristics of the emergent waters from the eleven acid mine drainage (AMD) study sites. Each site contained a terraced iron formation (TIF), either naturally occurring or engineered into an AMD passive treatment system. Values represent mean ± one standard deviation for n sampling events.

Parameter	United States – Appalachian region								Spain – Rio Tinto		
	Natural Sites					Engineered Sites			IPB		
	Brubaker run – BR	Scalp level – SL	Sulphur run – SR	Summerlee – SUM-N	Upper red Eyes – UR	Dents run – DR	Greens run – GR	Summerlee – SUM-E	La Zarza – LZP	Peña del Hierro – PDH	Rio Tintillo – RTL
Temp (°C)	11.0 ± 0.26	13.3 ± 0.67	10.4 ± 0.15	14.6 ± 0.64	9.38 ± 0.46	11.2 ± 12.6	14.5 ± 7.5	17.3 ± 5.0	26.5 ± 0.4	16.9 ± 2.1	24.3 ± 0.3
DO (mg/L)	0.06 ± 0.05	0.30 ± 0.06	0.14 ± 0.03	0.53 ± 0.6	0.18 ± 0.04		9.1 ± 2.2	5.3 ± 1.8	1.18 ± 0.8	2.75 ± 3.66	2.6 ± 3.1
ORP (mV)	348 ± 37	386 ± 39	315 ± 34	194 ± 49	284 ± 41	440 ± 19	465 ± 36	364 ± 41	323 ± 14	423 ± 28	368 ± 8.5
Conductivity (uS)	1690 ± 236	2010 ± 24	859 ± 41	1890 ± 147	2647 ± 44		1270 ± 816	2440 ± 220	7440 ± 395		18,900 ± 117
pH	3.37 ± 0.15	2.89 ± 0.08	3.48 ± 0.07	4.32 ± 0.64	4.04 ± 0.03	2.47 ± 0.08	3.13 ± 0.88	3.38 ± 0.88	3.13 ± 0.04	2.36 ± 0.12	2.96 ± 0.01
Dissolved total Fe (mg/L)	118 ± 27.9	97.4 ± 9.43	105 ± 6.4	278 ± 57	395 ± 8.4	302 ± 32	379 ± 331	236 ± 64	2930 ± 294	1220 ± 32	2640 ± 151
Dissolved Fe(II) (mg/L)	114 ± 28.4	92.3 ± 11.9	102 ± 6.5	275 ± 57	383 ± 20	135 ± 27	210 ± 166	230 ± 75	2740 ± 229	1090 ± 61	2310 ± 50
Al (mg/L)	11.6 ± 1.6	19.4 ± 0.4	16.5 ± 3.1	20.3 ± 1.3	55.6 ± 2.9	96 ± 3.4	96 ± 125	24.4 ± 8.14	245 ± 32	137 ± 7.3	1940 ± 45
Mn (mg/L)	34.5 ± 10.4	3.3 ± 0.1	14.6 ± 3.3	15.45 ± 0.61	105 ± 11	16.8 ± 0.66	3.82 ± 4.59	14.1 ± 1.32	60.4 ± 7.2	14.4 ± 0.33	314 ± 17
Co (mg/L)	0.69 ± 0.15	0.045 ± 0.003	0.64 ± 0.12	0.22 ± 0.01	3.82 ± 0.36	0.24 ± 0.00	0.32 ± 0.39	0.23 ± 0.04	1.12 ± 0.08	1.01 ± 0.04	9.6 ± 0.35
Ni (mg/L)	1.47 ± 1.10	0.16 ± 0.06	1.67 ± 1.23	0.48 ± 0.24	9.01 ± 6.07	0.56 ± 0.008	1.26 ± 1.71	0.33 ± 0.07	0.68 ± 0.07	0.05 ± 0.005	5.72 ± 0.18
Zn (mg/L)	1.75 ± 0.32	0.23 ± 0.03	2.13 ± 0.39	0.39 ± 0.02	12.2 ± 0.66	1.02 ± 0.02	1.17 ± 1.51	0.46 ± 0.04	46.4 ± 8.96	54.2 ± 9.4	385 ± 127
SO_4^{2-} (mg S/L)	381 ± 89	429 ± 34	212 ± 44	547 ± 37	903 ± 100	655	496 ± 634	549 ± 8	2530	1180	8190
Si (mg/L)	10.4 ± 0.3	16.5 ± 1.14	14.4 ± 1.2	14.2 ± 0.16	13.9 ± 0.21	38.9 ± 1.5	23.4 ± 26.4	16.8 ± 2.1	52.3 ± 0.29	52.1 ± 3.5	55.3 ± 5.1
PO_4^{3-} (mg P/L)	1.32 ± 1.86	1.3 ± 1.7	1.5 ± 2.1	1.10 ± 1.56	2.95 ± 3.84	<.05	7.16 ± 10.1	0.11 ± 0.11	1.62	0.5	3.81
n (field chemistry)	7	4	5	5	5	3	5	4	2	2	2
n (trace metals)	3	2	2	2	2	2	2	2	2	2	2
Mean Acidity (mg/L as $CaCO_3$)[*]	360	357	325	642	1220	1420	1410	609	6910	3310	16,400

[*] Acidity calculated according to (Kirby and Cravotta, 2005).

Table 2
Physical characteristics of the eleven acid mine drainage (AMD) study sites, and summary of Fe(II) oxidation kinetics measured in the field.

Parameter	United States – Appalachian Bituminous Coal Basin								Spain – Iberian Pyrite Belt		
	Natural Sites					Engineered sites					
	Brubaker run – BR	Scalp level – SL	Sulphur run – SR	Summerlee – SUM-N	Upper red eyes – UR	Dents run – DR	Greens run – GR	Summerlee – SUM-E	La Zarza – LZP	Peña del Hierro – PDH	Rio Tintillo – RTL
GPS location (lat/long)	40°37'1.42"N 78°28'35.76"W	40°14'43.72"N 78°51'33.18"W	40°18'25.91"N 78°44'5.06"W	38°0'18.06"N 81°9'29.04"W	40°14'27.07"N 78°44'25.42"W	41°20'26.66"N 78°22'18.54"W	39°30'19.38"N 79°41'53.25"W	38°0'19.39"N 81°9'28.68"W	37°42'22.70"N 6°51'48.38"W	37°43'30.41"N 6°33'21.62"W	37°42'31.86"N 6°37'14.06"W
Linear TIF Length (m)	70	65	50	8	275	188	140	90	747	244	796
$k_{1st,field}$ (min^{-1})	0.070 ± 0.032	0.399 ± 0.132	0.066 ± 0.039	0.034 ± 0.015	0.038 ± 0.004	0.048 ± 0.003	ND	0.068 ± 0.033	0.003 ± 0.001	0.028 ± 0.003	0.01 ± 0.003
$k_{zero,field}$ (mol/L ∗ s) ∗ 10^7	16.0 ± 6.10	81.3 ± 39.0	21.6 ± 10.2	29.1 ± 17.0	14.3 ± 3.40	8.60 ± 0.20	ND	36.3 ± 22.6	13.1 ± 9.40	67.9 ± 16.2	30.7 ± 1.10
n	5	4	3	4	3	3	–	3	2	2	2

The laboratory flow-through sediment reactors were modeled as tanks-in-series (TIS) to determine the pseudo first-order rate constant for Fe(II) oxidation ($k_{1st,lab}$). A conservative conductivity tracer (NaCl, 1410 μS) was injected into de-ionized water as a pulse input and measured every 30 s with the flow-through reactor operated at an 8 h residence time (residence time of the Fe(II) oxidation experiments). The conductivity results were analyzed using an exit age distribution ($E(\theta)$) to determine the non-ideality of the reactors (Crittenden et al., 2012). A TIS model was used to analyze the conductivity exiting the reactor according to:

$$E(\theta) = \frac{n(n\theta)^{n-1}}{(n-1)!} * \exp^{n\theta} \tag{3}$$

where θ was the normalized independent time variable, $E(\theta)$ was the exit age distribution, and n was the theoretical number of continuously stirred tank reactors (CSTR) in series. Theoretically, when $n = 1$, the reactor behaves as an ideal CSTR and as n approaches ∞, the reactor behaves as an ideal plug-flow reactor (PFR).

The conductivity tracer was performed with an empty reactor and repeated with a piece of non-reactive porous media (sponge) in the reactor. The best fits for the tracer breakthrough curves occurred with n ranging from 2 to 4 with an empty or filled reactor (Supplemental-3). A lower n value better modeled the tail of the tracer curve, while a higher n value better fit the rising portion of the tracer curve. An n value of 3 was selected for kinetic modeling as a compromise best-fit parameter.

Laboratory experiments were conducted using sediment and water collected from seven of the US sites (BR, SL, SR, SUM-N, UR, DR, and SUM-E). Sediment reactors similar to those described by Brown et al. (2010) used intact pieces of surficial sediments and emergent site water to measure rates of Fe(II) oxidation. Water height above the sediments was previously found to affect the rate of Fe(II) oxidation (Brown et al., 2010), therefore, water column height was fixed at 1.5 cm above the sediments. To maintain this fixed water column height, the water volume in each reactor varied slightly. Water volume was measured for every reactor and the flow rate was adjusted to maintain a hydraulic residence time of 8 h for all reactors. Water samples were collected from the inflow and outflow at the start of the experiment (time = 0), and after select pore volumes of fluid had been pumped through the reactors. Samples were immediately measured for pH (Mettler Toledo-InLab* Mini pH Electrode) and ORP (Mettler Toledo-InLab*⁻ Redox Mini Electrode), filtered (0.2 μm), and filtrate was added into either 0.5 M HCl or 0.5 M hydroxylamine–HCl for determination of dissolved Fe(II) and dissolved total Fe(T), respectively, using the ferrozine assay (Stookey, 1970). Experiments were run in triplicate for 48–64 h and conducted in parallel with duplicate no-sediment control reactors. At the conclusion of each experiment, a single sediment reactor was re-started to measure pH and ORP continuously, in real-time within the reactor. Electrodes were located near the outflow drain, configured to record samples every 10–30 s for the entire duration of the experiment (up to 60 h), and were relayed and stored on a laptop computer.

Determination of laboratory Fe(II) oxidation rate constants were based on first-order kinetics. Once steady-state conditions were established in the reactor (i.e., when [Fe(II)]$_{out}$/[Fe(II)$_{in}$ remained constant), the first-order model was calculated according to:

$$[Fe(II)_{out}] = \frac{[Fe(II)_{in}]}{(1 + k_{1st*H})^n} \tag{4}$$

where k_{1st} was the first-order laboratory Fe(II) oxidation rate constant (min^{-1}), [Fe(II)$_{in}$] was the steady-state inlet concentration of dissolved Fe(II) (M), [Fe(II)$_{out}$] was the steady-state outlet concentration of dissolved Fe(II) (M), n was the equivalent number of CSTR

tanks in series (from Eq. (3), set constant to $n = 3$), and θ_H was the hydraulic residence time (min). Laboratory Fe(II) oxidation rate constants were normalized to reactor sediment mass and viable biomass concentrations according to:

$$k_{1st,lab} = \frac{k_{1st}}{m * X} \tag{5}$$

where $k_{1st,lab}$ was the normalized first-order laboratory rate constant (min^{-1} pmols-PLFA^{-1}), m was the sediment mass in the reactor (g), and X was the viable (active) sediment biomass concentration (pmols-PLFA g^{-1} sediment).

2.4. Analytical techniques

Dissolved Fe(II) and dissolved total Fe(T) (after reduction by hydroxylamine–HCl) were determined using the ferrozine assay with samples preserved with HCl. Dissolved Fe(III) concentrations were determined from the difference of dissolved total Fe(T) and dissolved Fe(II) measurements. Dissolved metals (Al, Co, Mn, Ni, Si, Zn), metalloids (As), and non-metals (Se) were analyzed on a Perkin–Elmer Optima 5300 ICP-AES with samples that had been preserved with HNO$_3$. Concentrations of As and Se were below detection limits for all US sites (50 μg/L). Sulfate was measured spectrophotometrically by barium sulfate precipitation with chemically unpreserved samples (Hach Method 8051).

Upon completion of the laboratory experiments, approximately 50 wet grams of sediment were immediately collected into whirl-pak® bags and stored at −80 °C to minimize degradation of phospholipid fatty acids (PLFA). Samples were shipped on dry ice overnight and analyzed for PLFA by Microbial Insights, Inc. (Rockford, TN, US). PLFA measurements were performed only with sediments collected from the seven US sites used in the laboratory flow-through experiments. Upon cell death, membranes rapidly decay, and the concentration of total PLFAs represents the active or viable biomass concentration in the sample. The abundance of each type of PLFA provides information on microbial community structure. Active biomass concentrations (pmols-PLFA g^{-1} sediment) were used to normalize laboratory Fe(II) oxidation rates between sites (Eq. (5)). Upon arrival at Microbial Insights, sediments were thawed and lipids were extracted using a one-phase chloroform–methanol-buffer following a modified Bligh and Dyer method (White et al., 1979). Recovered lipids were fractionated into neutral lipids, glycolipids, and polar lipids using disposable silicic acid columns. The polar lipid fraction was transesterified by mild alkali methanolysis to recover the PLFAs as fatty acid methyl esters. PLFAs were determined on a gas chromatograph–mass spectrometer with electron ionization.

3. Results and discussion

3.1. Field sampling results

Because of the differences in acid-generating source rock, surrounding geologic strata, physical site conditions and the hydrogeological flow path from the source to the emergent discharge, water chemistry varied between all the sites (Table 1). Water chemistry for the few sites studied in each geologic region as compared to larger water chemistry databases are provided in Supplemental-4. Based on a simple rank analysis, our selected sites contained lower pH values and higher concentrations of dissolved total Fe(T) compared to median values in both regions. Sites were selected with low concentrations of dissolved oxygen (DO), low oxidation–reduction potentials (ORP), and a high proportion of dissolved Fe(II) to dissolved total Fe(T). These geochemical conditions were intentionally selected to study sites where low-pH Fe(II)

oxidation was a dominant process downstream of the emergent springs.

Seasonal variations in water chemistry at any site may have been caused by changes in water table elevations that could impact pyrite oxidation (Nordstrom, 2011), and/or by complexities in underground conditions (Price, 2003). The temperature of emergent AMD varied between sites and reflected differences in site-specific hydrogeology and hydrogeochemistry. For the natural TIF sites in the US, emergent DO was typically less than 0.5 mg/L. Higher concentrations of DO were measured at the engineered sites in the US (5–9 mg/L) and at the Spanish sites (1–3 mg/L). Higher concentrations of DO and lower ratios of Fe(II)/Fe(T) were measured at these sites because the emergence (i.e., exposure to atmospheric P_{O2}) occurred upstream (e.g., in partially flooded mines or partially saturated spoils piles) of our most upstream sampling location.

Measured trace metal concentrations for all sites were above chronic Ambient Water Quality Criteria (AWQC) for aquatic life, which are as follows (μg/L): Al – 87, Cd – 0.25, Co – 3.06, Cu – 11.8, Fe – 1000, Mn – 80.3, Ni – 52, Pb – 3.2, Zn – 106 (Seal et al. 2010, US EPA 2013). The highest concentrations of Al for the US sites were measured at GR (96 ± 125 mg/L), DR (96 ± 3.4 mg/L), and UR (56 ± 2.9 mg/L). The IPB sites (RTL, LZP, and PDH) contained metal concentrations an order of magnitude higher than sites in the US. Notably, dissolved total Fe(T) concentrations ranged from 1223 to 2928 mg/L. Rio Tintillo (RTL) contained the highest concentrations of Al (1942 mg/L), Mn (314 mg/L), Co (9.6 mg/L), Ni (5.7 mg/L) and Zn (385 mg/L). Lower trace metal concentrations were observed at LZP and PDH, yet generally still exceeded any concentrations observed at US sites. Theoretical mean acidity values (calculated according to (Kirby and Cravotta, 2005)) for the US sites ranged from 325 to 1422 mg/L as CaCO$_3$, while calculated mean acidities for the IPB sites ranged from 3307 to 16,410 mg/L as CaCO$_3$. Periods of high flow substantially diluted the AMD at GR, which resulted in variable iron concentrations ([Fe(II)] = 210 ± 166 mg/L, [Fe(T)] = 379 ± 331 mg/L), trace metals, and sulfate (Table 1). Compared to cation and anion concentrations, the pH and ORP were less susceptible to seasonal changes at GR (pH – 3.13 ± 0.88, ORP – 465 ± 36 mV). Due to their physical proximity, emergent AMD from SUM-N and SUM-E had similar geochemistry and were presumably originating from the same coal refuse pile. The natural TIF sites, BR, SL, SR and UR, displayed relatively consistent emergent chemistry throughout all sampling events.

Longitudinal geochemical transects across the TIFs were measured on several seasonal sampling events for pH, ORP, DO, temperature, trace metals, and Fe speciation. For the majority of these sites, the general geochemical trends were for DO and ORP to increase, dissolved Fe(II) to decrease, dissolved total Fe(T) to decrease slightly, temperature to approach ambient conditions, and trace metals to remain unchanged. The trends for pH across the TIFs could not be generalized. For example, pH tended to decrease across four of the five natural TIFs in the US (Fig. 2), one of the three engineered TIFs (Fig. 3), and two of the three TIFs in the IPB (Fig. 4). Microbial-catalyzed Fe(II) oxidation can produce either soluble Fe(III) (Eq. (6)) or insoluble Fe(III) (Eq. (7)) according to:

$$Fe^{2+} + \frac{1}{4}O_2 + H^+ = Fe^{3+} + \frac{1}{2}H_2O \tag{6}$$

$$Fe^{2+} + \frac{1}{4}O_2 \text{ (g)} + \frac{7}{32}SO_4^{2-} + \frac{17}{16}H_2O$$
$$= \frac{25}{16}H^+ + \frac{1}{8}Fe_8O_8(SO_4)_{1.75}(OH)_{4.5} \tag{7}$$
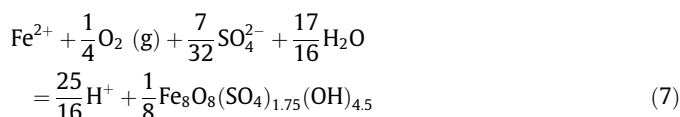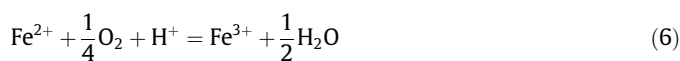
where $Fe_8O_8(SO_4)_{1.75}(OH)_{4.5}$ represents a nominal stoichiometry for schwertmannite (Regenspurg et al., 2004). In Eq. (6), acidity is
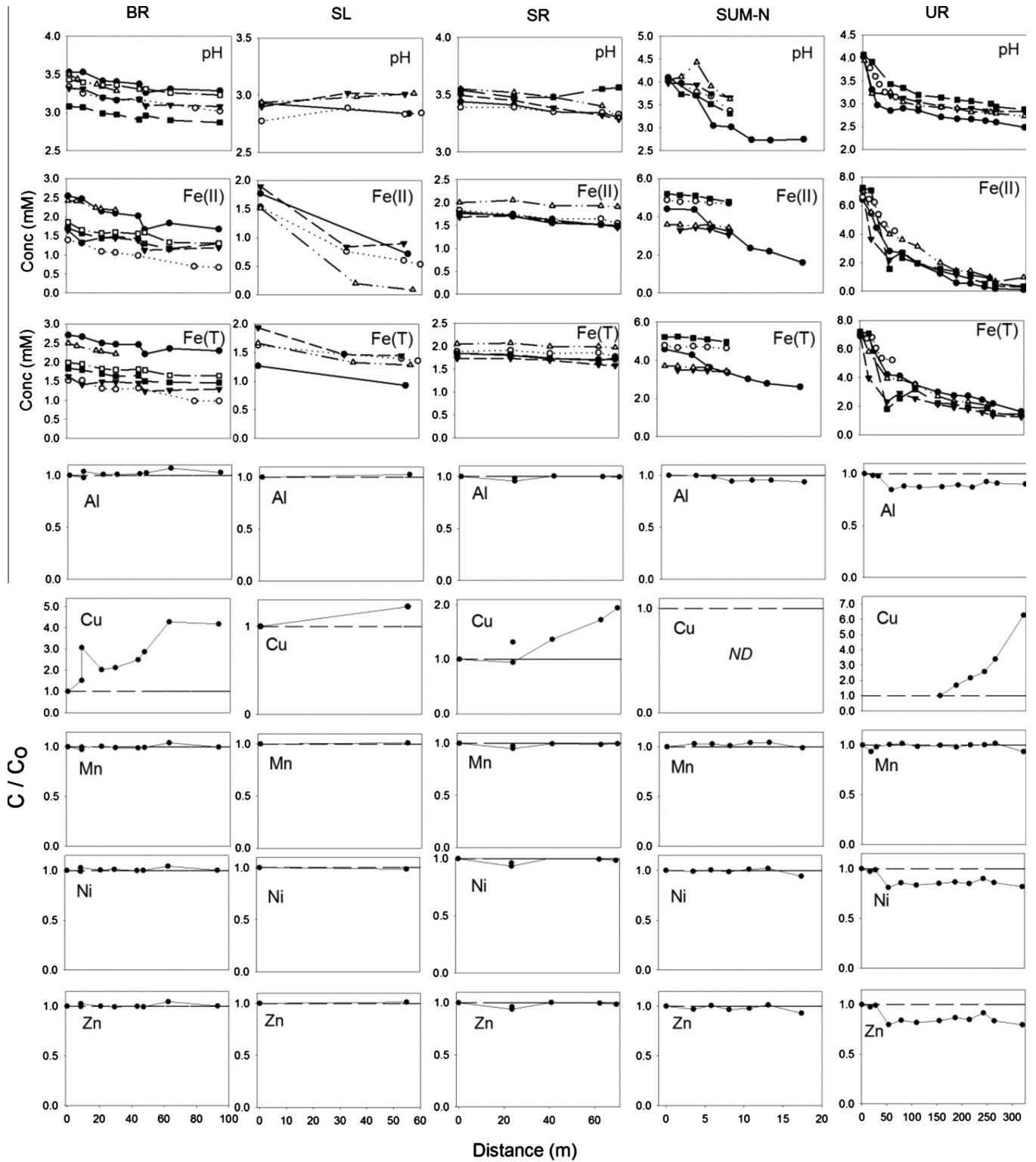
Fig. 2. Longitudinal geochemical transects for natural TIF sites in the US for pH, Fe speciation (mM), and trace metals. Data were collected 3–6 time at any given site. Trace metals are presented as the ratio of C/C_o to show changes relative to emergent metal concentrations. Trace metal transects were collected once.

consumed while in Eq. (7) acidity is produced. At virtually all sites, both dissolved Fe(II) and dissolved total Fe(T) decreased, and dissolved Fe(III) increased, indicating that both Eqs. (6) and (7) were operative. The removal of soluble Fe(III) is controlled by pH, the solubility of schwertmannite, and the kinetics of schwertmannite precipitation.

For presentation purposes, results have been divided into natural TIFs in the US (Fig. 2), engineered TIFs in the US (Fig. 3) and natural TIFs in Spain (Fig. 4). Trace metals across the TIFs were collected on one occasion, while pH and Fe speciation were collected two to six times. Comparisons of geochemical transects highlight important distinctions between the type of TIF (natural versus engineered)
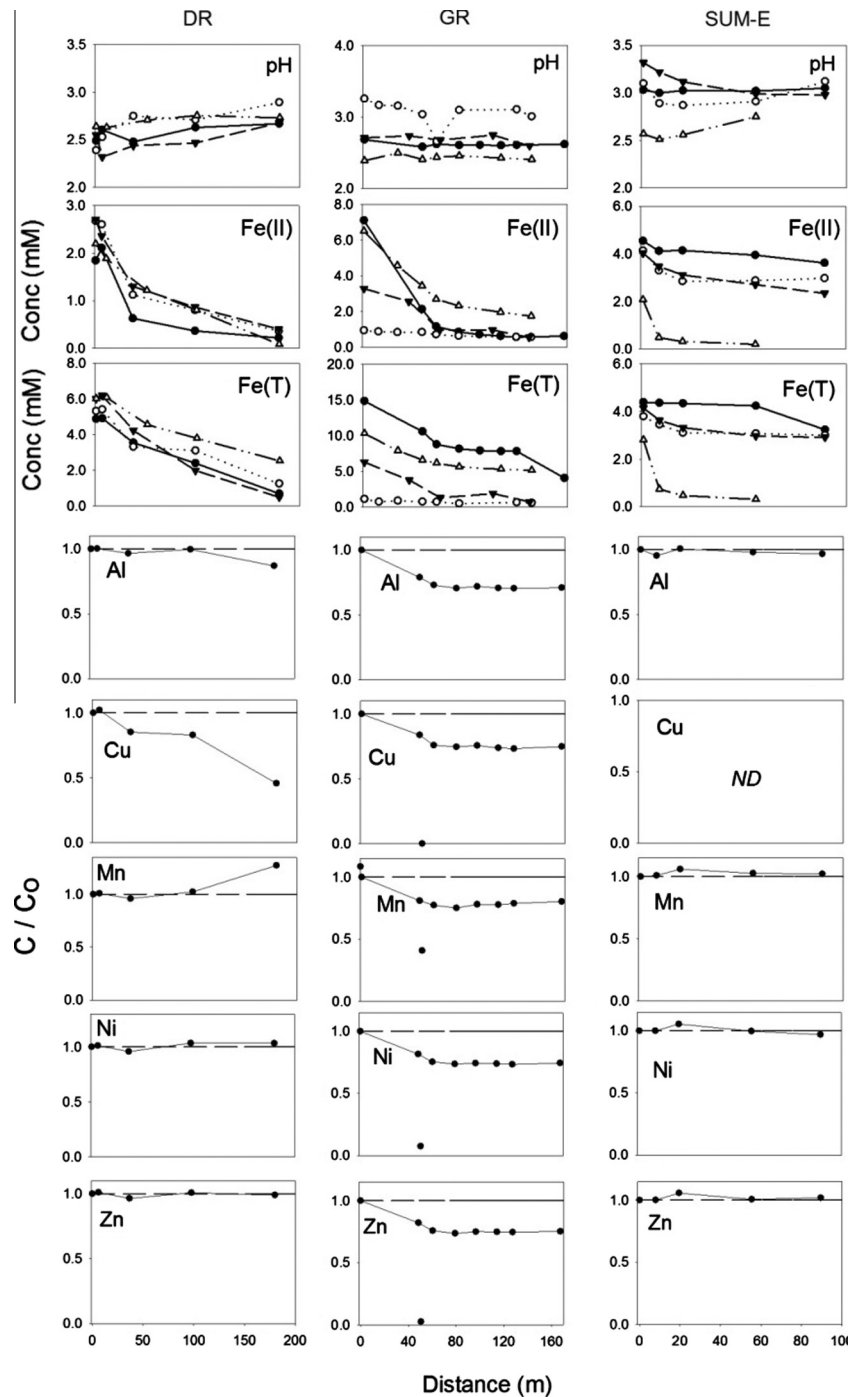
Fig. 3. Longitudinal geochemical transects for engineered TIF sites in the US for pH, Fe speciation (mM), and trace metals. Data were collected 4–5 times at any given site. Trace metals are presented as the ratio of C/C$_o$ to show changes relative to emergent metal concentrations.

and AMD source (e.g., coal versus metal mines) on pH, Fe speciation, and trace metal mobility. These transects are plotted as a function of distance from the emergent AMD sources and some variations in geochemistry were dependent on the emergent flow rate and the local water velocity.

Longitudinal geochemical transects across most natural TIFs in the US displayed behavior consistent with Eq. (7) where dissolved Fe(II) and dissolved total Fe(T) decreased along with pH. Scalp Level (SL) was the one natural TIF site where pH did not drop but instead tended to increase. SL also had a lower emergent pH (2.51–2.90) as compared to the other natural TIFs (typically between pH 3.0 and

4.0). Even so, dissolved Fe(II) concentrations decreased from 50% to 90% of emergent Fe(II) concentrations while dissolved total Fe(T) decreased to a much lower extent. The geochemical transect at SL, therefore, displayed behavior more consistent with Eq. (6). Trace metal (Al, Cu, Mn, Ni, Zn) behavior for all natural TIF sites in the US were relatively similar (Fig. 3). In general, there was no significant removal of trace metals at any natural TIF. Decreases in Al, Mg, Ni, S and Zn were measured at UR. Decreases in metal concentrations at UR were likely caused by dilution with additional base flow entering this large TIF. Assuming concentrations of S and Fe from AMD sources are strongly correlated, and assuming S
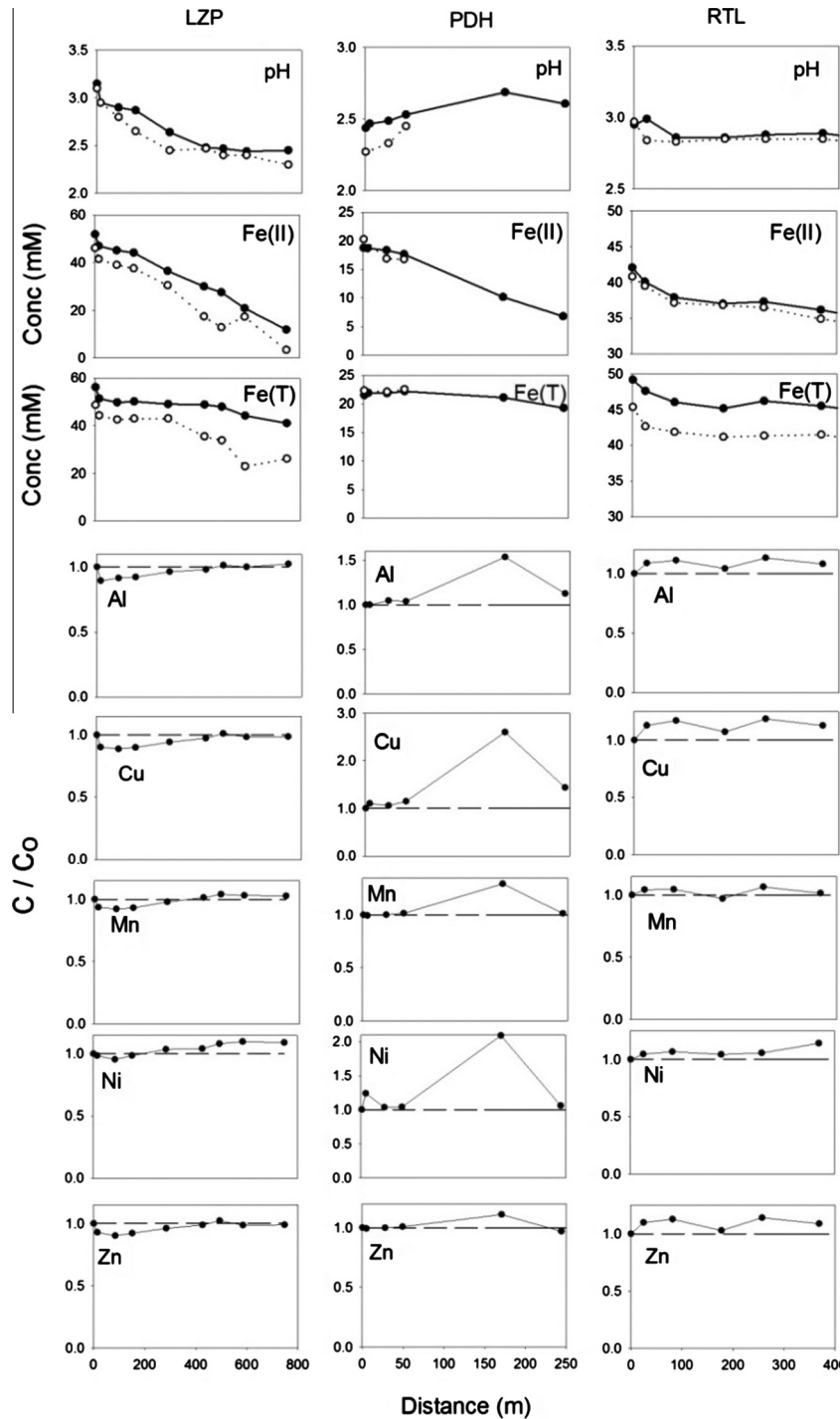
Fig. 4. Longitudinal geochemical transects for TIF sites in the IPB for pH, Fe speciation (mM), and trace metals. Data were collected twice at all sites. Trace metals are presented as the ratio of C/C$_o$ to show changes relative to emergent metal concentrations.

and Mg act as conservative elements, we found that S and Mg decreased ~20% compared to their emergent concentrations suggesting base flow dilution. Increasing soluble Cu concentrations were measured at four sites, possibly due to decreased adsorption affinity of Cu to schwertmannite (Webster et al., 1998) and/or enhanced metal solubility of Cu-bearing minerals at lower pH values.

Longitudinal geochemical transects measured across engineered TIFs were rather variable (Fig. 3) compared to the natural TIF sites. Samples were collected from engineered channels at GR

(concrete) and DR (limestone gravel), while SUM-E was designed to promote sheet flow across its clay-based "raceway". In contrast to natural sites, emergent AMD at the engineered sites was partially oxidized due to modified hydrogeochemical conditions at each site. Emergent pH values ranged from 2.4 to 3.4. On one occasion, higher pH values were observed at GR (pH 4.5; high flow condition) and SUM-E (pH 4.9; low flow condition) (transect data not shown in Fig. 3 and not included in Table 1). For three sampling events at GR, pH values remained relatively constant across the TIF while both dissolved Fe(II) and dissolved total Fe(T) decreased
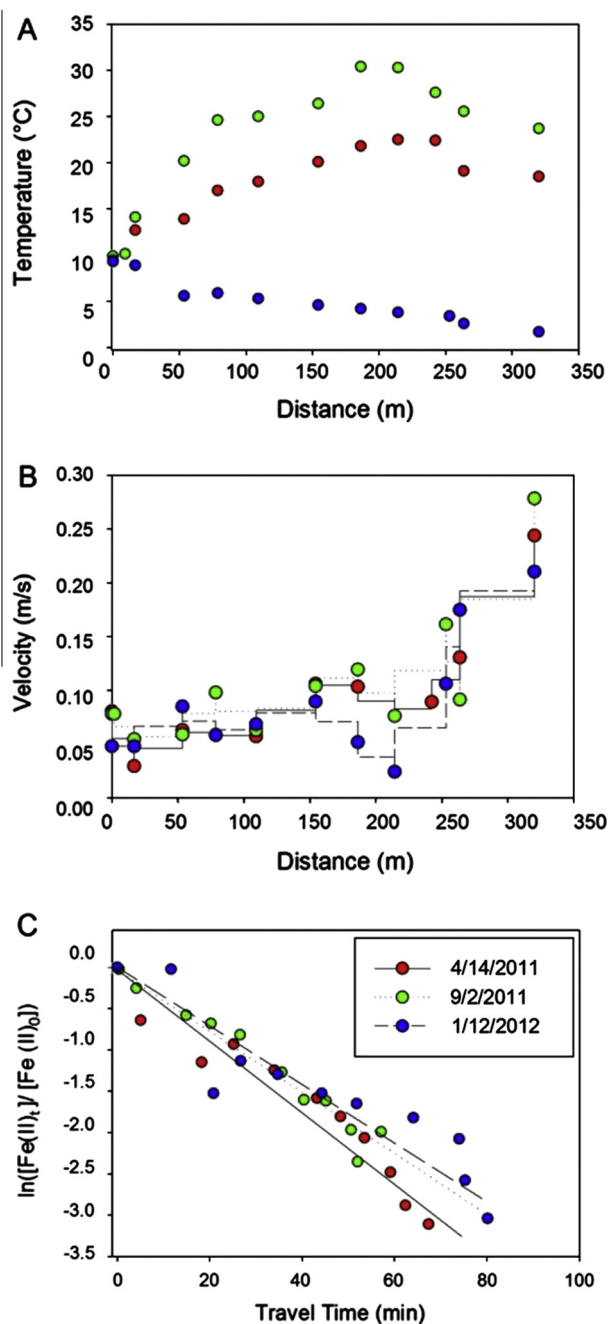
Fig. 5. Representative example from Upper Red Eyes (UR) showing data transformation of distance (m) to travel time (min) to calculate Fe(II) oxidation rates in the field. (A) Water temperature downstream of emergent AMD source. (B) Water velocity measured at discrete sampling locations (points) and the averaged velocity between any two sampling locations (lines). Travel times were calculated as the distance between two sampling locations divided by the averaged velocity. (C) Dissolved concentrations of Fe(II) versus cumulative travel time were used to calculate first-order Fe(II) oxidation rate constants. (For interpretation of the references to color in this figure legend, the reader is referred to the web version of this article.)

significantly. Dissolved concentrations of all trace metals (Al, Cu, Mn, Ni and Zn) at GR decreased approximately 30% compared to their emergent concentrations. Dilution from other point sources accounted for some of these decreases, as S and Mg decreased by ~20% compared to their emergent concentrations. We propose that additional trace metal removal was promoted by alkaline minerals in the concrete channel. While the pH at GR typically was less than 4, alkalinity generated via concrete dissolution could create

localized zones of higher pH that facilitated precipitation of dissolved Fe(III) and co-precipitation of trace metals into the Fe(III) minerals. Ca concentrations remained constant along the channel even while Mg concentrations decreased, demonstrating that Ca dissolution was occurring, thus supporting our interpretation.

Similar to GR, substantial amounts of dissolved Fe(II) and dissolved total Fe(T) were removed in the engineered channel at Dents Run (DR). While oxidative precipitation of schwertmannite (Eq. (7)) should produce acidity, dissolution of the limestone gravel in the shallow channel at DR buffered the pH of this system such that it actually increased slightly (from pH 2.5 to pH 2.8) along this transect. Increasing calcium concentrations measured across this TIF support this hypothesis. Concentrations of dissolved Fe(III) were found to be slightly over-saturated with respect to ferrihydrite and schwertmannite (Supplemental-5). At DR, Cu and Al were the only trace metal concentrations to decrease along this transect. The extent of Fe(II) oxidation and removal of dissolved total Fe(T) was lowest at the Summerlee-Engineered (SUM-E) site as compared to the other engineered TIF sites. SUM-E also displayed the most inconsistent geochemical behavior. Both of these results, limited and variable oxidative precipitation of Fe, were likely because this was a newly constructed TIF that has yet to "mature".

Longitudinal geochemical transects at the IPB sites were measured on two occasions, March and May 2012 (Fig. 4). In general, emergent pH values were lower in the IPB as compared to the US sites, ranging from pH 2.3 to 3.1. Emergent concentrations of dissolved Fe(II) and dissolved total Fe(T) at the IPB sites were almost an order of magnitude higher than any US site (1223–2928 mg/L). Therefore, even modest changes in the [Fe(II)]/[Fe(T)] ratio amounted to substantial masses of Fe deposited onto these TIFs. For all of the IPB sites, no metal was removed other than Fe, while slight increases in Cu, Ni and Zn were measured downstream of RTL and PDH (Fig. 4). At RTL, increased metal concentrations could have been caused by additional AMD sources entering the study reaches. Similar to Scalp Level in the US, the pH increased downstream of Peña del Hierro (PDH) while dissolved Fe(II) decreased 64% compared to the emergent concentration but dissolved total Fe(T) decreased only 8%.

3.2. Rates of Fe(II) oxidation in the field

A representative data set from Upper Red Eyes (UR) shows the successive transformation of field data, using stream velocities, to estimate $k_{1st,field}$ (Fig. 5). The emergent temperatures were fairly constant (~10 °C), while the downstream temperature gradients were controlled by the seasonal ambient temperature (Fig. 5A). Velocity measurements were averaged between sampling locations and were fairly consistent regardless of season for this site (Fig. 5B). Field rate constants were determined according to:

$$-d[\text{Fe(II)}]/dt = k_n^*[\text{Fe(II)}]^n \qquad (8)$$

where $n = 0$ and $n = 1$ represent the zero- and first-order rate expressions, respectively. The slopes of the lines in Fig. 5C were used to calculate the first-order rate constants for each sampling event. First-order Fe(II) oxidation rate constants measured in the field ($k_{1st,field}$) for UR ranged from 0.035 min^{-1} (in January 2012) to 0.044 min^{-1} (in April 2011) (Fig. 5C).

For some field sites, the physical assumptions for our kinetic stream reach model were not met. We assumed the stream reach functioned as a plug flow reactor with no other inputs of flow or dissolved Fe(II). Rates of Fe(II) oxidation were not calculated at GR because additional point sources discharged directly into this engineered TIF, invalidating our model assumptions. At the largest natural TIF sites (UR, RTL), additional seeps and base flow did enter the systems but never from obvious point sources. If these diffuse

sources contained elevated concentrations of Fe(II), then our measured (i.e., apparent) field rates would be less than the actual rates. Conversely, if these diffuse sources contained relatively low concentrations of Fe(II), then our measured field rates would be greater than the actual rates. Assuming S acts as a conservative proxy for Fe, base flow dilution did occur at UR but did not occur at RTL. Thus, the measured rates at UR could be greater than the actual rates. Considering uncertainties with respect to model assumptions and hydrogeochemical variability between sampling events, the relative standard deviations of the field rates measured at UR and RTL were relatively low compared to all 10 sites (Table 2) providing confidence in these rate measurements. The measured field rates at UR and RTL were also near the median values for each region, neither exceptionally fast nor slow. Finally, because we tended to measure water velocity in stream reaches where our tracer was swept along via advective transport, our calculated travel times could be biased as relatively short compared to all the water flowing across each TIF. Thus, all of our calculated kinetic constants could be biased as relatively fast when compared to other studies. While we recognize the difficulty in measuring geochemical kinetics in the field, we propose that all of our rates are comparable within this study because we used identical methods at all sites.

Field-based Fe(II) rate constants and physical site characteristics are presented in Table 2. Physical site parameters (transect distance, surface area, and average slope) were obtained using geospatial processing of 3D digital elevation maps (DEM) in ArcGIS. Physical conditions were variable between sites. For example, UR was a relatively large TIF site that can be observed from satellite imagery, while SUM-N was only ~8 m in length. The fastest $k_{1st,field}$ for any natural US site was 0.497 min^{-1} (SL in April 2011) while the slowest $k_{1st,field}$ was 0.030 min^{-1} (SUM-N in December 2011). Excluding SL, the mean value for $k_{1st,field}$ from natural TIF sites in the US ranged from 0.035 to 0.070 min^{-1}.

Uncertainty with these kinetic analyses was most likely associated with the transformation of the independent variable of distance to travel time. Seasonally variable velocity measurements and the validity of assumptions used to calculate the average velocity between two sampling points could affect this transformation. Considering variable physical site characteristics, geochemical variability, and error and uncertainty associated with the first-order rate model, the calculated rate constants from the different sites were remarkably similar. First-order rate constants determined on each sampling event are provided in Supplemental-6. Rates of Fe(II) oxidation on engineered TIFs were comparable to rates of Fe(II) oxidation on natural TIF sites in the US (Table 2).

First-order rate constants of Fe(II) oxidation calculated for the IPB sites were ~10 times slower than first-order rate constants calculated at the US sites. First-order rate constants ranged from 0.003 to 0.01 min^{-1} (Table 2). However, zero-order Fe(II) oxidation rates ($k_{zero,field}$) calculated for the IPB sites were comparable to zero-order rates calculated for the US sites. In the IPB, $k_{zero,field}$ ranged from 13.1×10^{-7} to 67.9×10^{-7} mol L^{-1} s^{-1}. At the US sites, mean $k_{zero,field}$ ranged from 8.60×10^{-7} to 81.3×10^{-7} mol L^{-1} s^{-1}. It should be noted that interpretative discrepancies can be caused by the rate model used to describe the field results. First-order rate constants from the IPB sites may have been slower because of the higher conductance and trace metal concentrations in the waters of that geographic region (Table 1).

The fastest $k_{1st,field}$ were measured at sites with the lowest emergent pH values in both the US and the IPB (Fig. 6A). First-order rate constants grouped into distinct sets based on their geographic region. These correlations are consistent with the rate law for biotic Fe(II) oxidation proposed by Kirby et al. (1999) where the rate was proportional to [H$^+$] (Eq. (2)). $k_{1st,field}$ were also fastest at sites where pH increased across the TIF (Fig. 6B). The change in pH across each TIF (ΔpH) was calculated as the pH at the bottom of the site minus the pH at the emergent spring at the top of site. If the pH increased across the site (ΔpH > 0), this would provide indirect evidence for the consumption of H$^+$ associated with the production of soluble Fe^{3+} (Eq. (6)). Similarly, if the pH decreased across the site (ΔpH < 0), this would provide indirect evidence for the production of H$^+$ associated with the precipitation of an Fe(III) mineral such as schwertmannite (Eq. (7)).

3.3. Rates of Fe(II) oxidation in the laboratory

Representative results from flow-through low-pH Fe(II) oxidation experiments using sediments and AMD from UR displayed a rapid decrease in the [Fe(II)$_{out}$]/[Fe(II)$_{in}$] ratio between 0 and 10 h (Fig. 7A). No Fe(II) oxidation was observed in no-sediment control reactors, confirming that biotic processes were responsible for oxidizing Fe(II) within the sediment reactors. In similar previous experiments, Brown et al. (2010) showed that no Fe(II) oxidation occurred in gamma-irradiated, sterilized sediments. Approximately 24 h into the experiment (equivalent to three pore volumes), the [Fe(II)$_{out}$]/[Fe(II)$_{in}$] ratio began to achieve a pseudo steady-state condition. Fe(II) oxidation rates in laboratory experiments were calculated and averaged over the whole duration of this pseudo steady-state period. Measurements of pH collected on a much more intensive time scale also demonstrated that pseudo steady-state conditions with respect to pH were established within 10 h (Fig. 7B). Steady-state conditions with respect to ORP took longer to establish, possibly because non-ideal mixing affected oxygen transfer (Fig. 6B).

Rate constants were normalized based on sediment mass and biomass concentration. The biomass-normalized Fe(II) oxidation rates ($k_{1st,lab}$) ranged from 10×10^{-11} to 68×10^{-11} min^{-1} pmol-PLFA^{-1} (Table 3). The fastest laboratory rate of Fe(II) oxidation was measured using sediments and AMD collected from SL. Relative standard deviations (RSD = standard deviation/mean value * 100%) were high in these experiments. For example, the RSD for the SL sediment experiments was 54%, the RSD for the SUM-E sediment experiments was 58%, and the RSD values for the remaining five sediments were <36%. Error and uncertainty associated with these experiments were most likely associated with sediment heterogeneity and non-ideal mixing in the reactors.
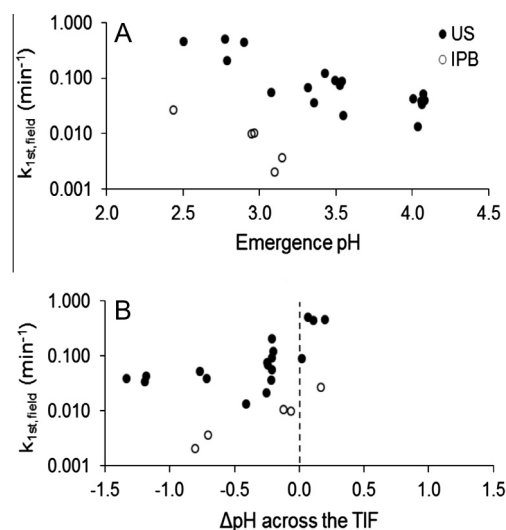
Fig. 6. Observed first order field Fe(II) rate constants ($k_{1st,field}$) at the US and IPB field sites displayed with (A) emergent pH and (B) ΔpH across the TIF. Positive values for ΔpH denote a net pH increase across the TIF and negative ΔpH values indicate a net pH decrease. Positive values for ΔpH are consistent with the oxidation of Fe(II) to soluble Fe(III) (Eq. (6)). Negative values for ΔpH are consistent with the oxidation of Fe(II) and precipitation of Fe(III) (Eq. (7)).
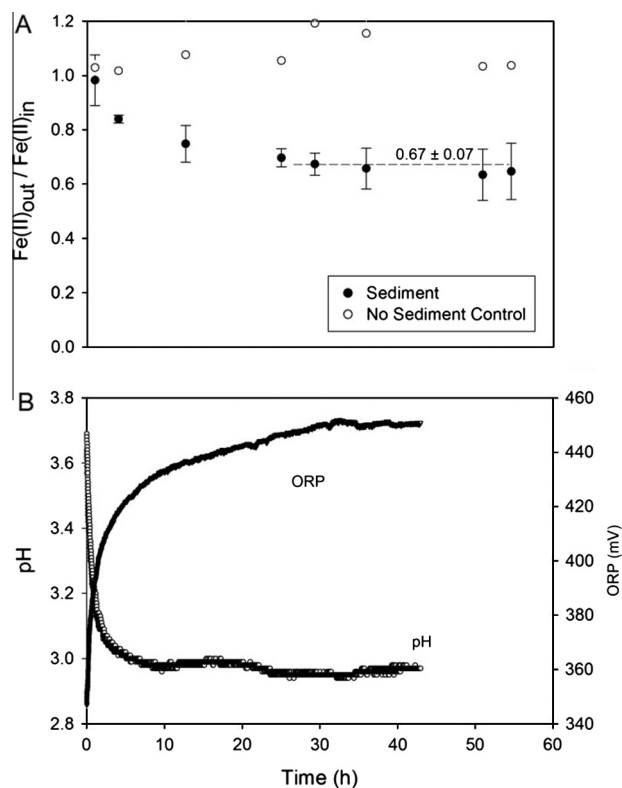
Fig. 7. Representative laboratory data for sediments and water collected from Upper Red Eyes (UR). (A) Laboratory rates of Fe(II) oxidation were calculated from concentrations of dissolved $Fe(II)_{out}/Fe(II)_{in}$ when pseudo steady-state conditions were established (dashed line). (B) Real-time pH and ORP results for sediments and water collected from UR. Real-time results for no-sediment controls showed no appreciable changes (data not shown).

The majority of the sediments had relatively low microbial diversity and contained a large abundance of proteobacteria and general PLFAs (Fig. 8). A complete PLFA profile for each site is provided in Supplemental-7. BR and SR contained the highest abundance of eukaryotes (10% and 6%, respectively), while SL contained the highest abundance of firmicutes (26%). There was a large range of biomass concentrations; DR contained the maximum (67,000 pmols-PLFA g^{-1} sediment) and SL the minimum (6500 pmols-PLFA g^{-1} sediment). Interestingly, SL had the highest observed field and lab Fe(II) oxidation rate constants, yet sediments collected from the site had the lowest active biomass concentration and a considerably different PLFA profile (i.e., much higher abundance of firmicutes, less abundance of proteobacteria). The other sites (UR, SUM-N, and SUM-E) contained similar biomass and abundances.

3.4. Environmental implications

Our results are consistent with several other studies that have reported Fe(II) oxidation rates. Zero-order oxidation rates from all eleven sites varied only by a factor of ~11 (Table 2), where $k_{zero,field}$ ranged from 8.60×10^{-7} to 81.3×10^{-7} mol L^{-1} s^{-1}. These values compare favorably with those reported by Brown et al. (2010) (0.6×10^{-7} to 1.6×10^{-7} mol L^{-1} s^{-1}), Kirby and Elder-Brady (1998) (1.0×10^{-9} to 3.3×10^{-6} mol L^{-1} s^{-1}), Nordstrom (1985) (3.6×10^{-7} to 9.7×10^{-7} mol L^{-1} s^{-1}) and Sánchez España et al. (2007a) (4.0×10^{-7} to 5.5×10^{-6} mol L^{-1} s^{-1}). First-order rate constants varied by a factor of ~130 between all eleven sites but were grouped much more closely when binned into their separate geographic regions. When considered as two separate data sets (one for US, one for IPB), $k_{1st,field}$ values increased with decreasing emergent pH (Fig. 6A). The fastest first-order rate constants also occurred at sites where the pH increased across the TIF (Fig. 6B), and little dissolved Fe(T) was removed from solution. Laboratory-based first-order rate constants were also fastest for sites where less dissolved

Table 3
Summary of Fe(II) oxidation kinetics measured in the laboratory for seven of the eleven study sites.

Parameter	United States – Appalachian Bituminous Coal Basin						
	Natural sites					Engineered sites	
	BR	SL	SR	SUM-N	UR	DR	SUM-E
Mass (g)	96	93	101	87	155	54	111
Biomass concentration (pmols PLFA g^{-1})	25,172	6464	20,124	18,678	20,117	66,871	10,258
Surface area (cm^2)	38	41	63	47	101	56	73
$k_{1st,lab}$ (min^{-1} $*$ pmol-PLFA^{-1}) $* 10^{11}$	18 ± 4	68 ± 37	14 ± 5	11 ± 2	10 ± 1	21 ± 4	31 ± 18
GDM (g Fe d^{-1} m^{-2})	5.0	2.6	3.0	8.7	7.7	6.6	5.1
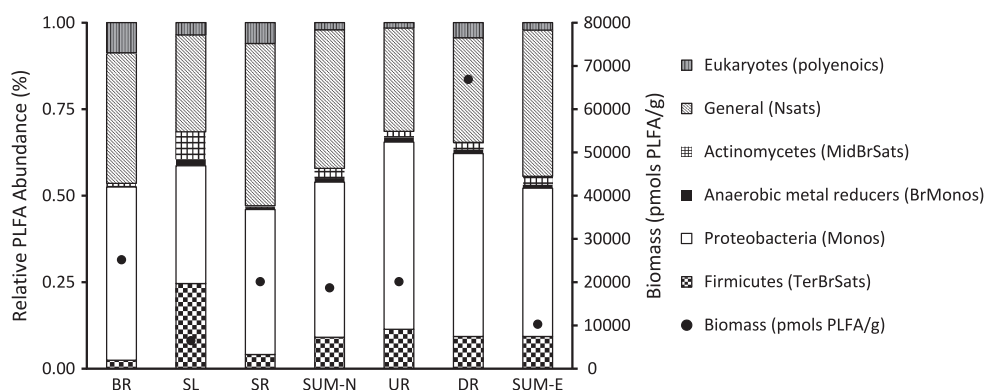
Fig. 8. Concentrations and distributions of phospholipid fatty acids (PLFAs) extracted from sediments used in laboratory experiments. The bar chart shows the relative distribution of each taxonomic group (%; left axis) and the filled circles show the total biomass concentration (pmols PLFA g^{-1}; right axis).

Fe(T) was removed from solution (Supplemental-8). In other words, faster Fe(II) oxidation rate constants occurred where less dissolved Fe(T) was removed from solution.

AMD passive treatment systems are often empirically sized on land area-based contaminant removal rates such as g Fe d^{-1} m^{-2} (Watzlaf et al., 2002; Ziemkiewicz et al., 1997). Using our flow-through laboratory sediment reactors we calculated area-based removal rates of 2.6–8.7 g Fe(T) d^{-1} m^{-2} (GDM) (Table 3). These results are consistent with Brown et al. (2010), who reported values of 3.4–6.3 GDM for similar laboratory reactors using sediments collected from several locations across the TIF at Upper Red Eyes (UR). In comparison, design guidelines for Fe removal from net-acidic coal mine drainage using aerobic wetlands range from 2 to 5 GDM (Hedin and Nairn, 1992). Our new data should support and solidify a design criteria of 4–8 GDM for low-pH Fe(II)-oxidizing TIFs.

The overarching goal of AMD treatment is neutralization of acidity and removal of metals. Therefore, an ideal treatment scenario would promote both Fe(II) oxidation and subsequent Fe(III) precipitation across a TIF. The engineered TIFs at GR and DR represent an ingenious (albeit serendipitous) modification to enhance the removal of Fe(T) and possibly other trace metals. Wider channels with lower water column depths will improve oxygen transfer and increase contact of AMD with the alkaline minerals lining the channel. Relatively low pH values were measured at GR and DR (2.4–3.1) yet substantial amounts of dissolved Fe(T) were removed from solution (Fig. 3). We propose that dissolution at the channel mineral-AMD interface created microenvironments with pH values higher than the bulk solution that promoted the precipitation of Fe(III). The relatively constant (or increasing) pH across the engineered TIFs at GR and DR was consistent with calcite dissolution balancing the acidity produced from Fe-hydrolysis and precipitation (Cravotta et al., 2004). Based on our field and laboratory results, the fastest rates of Fe(II) oxidation occurred in systems where relatively little Fe(T) was removed from solution. Therefore, we propose that natural and engineered features can be combined to maximize AMD treatment across a TIF. Natural TIFs would be retained to promote Fe(II) oxidation while a calcareous channel could be used to extend into an engineered TIF. This shallow channel would be similar to an oxidation ditch and distinct from a limestone bed. An oxidation ditch is shallow (0-cm bed depth with concrete, ~5-cm bed depth with gravel) as compared to a limestone bed (~1-m bed depth), and designed for open-channel flow as compared to flow through saturated porous media. This channel would not be intended to neutralize a large portion of the AMD acidity but instead serve as a substrate for Fe(II)-oxidizing bacteria and as an area for the accumulation of Fe(III) solids. Encouragingly, the armoring of the limestone at DR and the concrete at GR has not yet seemed to exert a negative effect on the performance of these engineering TIFs. The exact ratio of travel times across the natural and engineered sections would depend on site-specific conditions such as emergent geochemistry and land availability. This integration of natural and engineered TIFs will promote both Fe(II) oxidation and Fe(III) precipitation.

Acknowledgements

Appendix A. Supplementary material

Supplementary data associated with this article can be found, in the online version, at http://dx.doi.org/10.1016/j.apgeochem.2014.05.012.

References

Bigham, J.M., Schwertmann, U., Traina, S.J., Winland, R.L., Wolf, M., 1996. Schwertmannite and the chemical modeling of iron in acid sulfate waters. Geochim. Cosmochim. Acta 60, 2111–2121. http://dx.doi.org/10.1016/0016-7037(96)00091-9.

Brown, J.F., Jones, D.S., Mills, D.B., Macalady, J.L., Burgos, W.D., 2010. Application of a depositional facies model to an acid mine drainage site. Appl. Environ. Microbiol.. http://dx.doi.org/10.1128/aem.01550-10. AEM.01550-01510.

Burgos, W.D., Borch, T., Troyer, L.D., Luan, F., Larson, L.N., Brown, J.F., Lambson, J., Shimizu, M., 2012. Schwertmannite and Fe oxides formed by biological low-pH Fe(II) oxidation versus abiotic neutralization: Impact on trace metal sequestration. Geochim. Cosmochim. Acta 76, 29–44. http://dx.doi.org/10.1016/j.gca.2011.10.015.

Cánovas, C.R., Hubbard, C.G., Olías, M., Nieto, J.M., Black, S., Coleman, M.L., 2008. Hydrochemical variations and contaminant load in the Río Tinto (Spain) during flood events. J. Hydrol. 350, 25–40. http://dx.doi.org/10.1016/j.jhydrol.2007.11.022.

Chen, C.-J., Jiang, W.-T., 2012. Influence of waterfall aeration and seasonal temperature variation on the iron and arsenic attenuation rates in an acid mine drainage system. Appl. Geochem. 27, 1966–1978. http://dx.doi.org/10.1016/j.apgeochem.2012.06.003.

Cornell, R.M., Schwertmann, U., 1996. The Iron Oxides: Structure, Properties, Reactions, Occurence, and Uses, third ed. VCH, Weinheim, New York, Basel, Cambridge, Tokyo.

Cravotta, C.A., Kirby, C.S., District, N.C.C., 2004. Effects of abandoned coal-mine drainage on streamflow and water quality in the Shamokin Creek Basin, Northumberland and Columbia Counties, Pennsylvania, 1999–2001. US Department of the Interior, US Geological Survey.

Crittenden, J.C., Trussell, R.R., Hand, D.W., Howe, K.J., Tchobanoglous, G., 2012. MWH's Water Treatment: Principles and Design. Wiley.

DeSa, T., Brown, J., Burgos, W., 2010. Laboratory and field-scale evaluation of low-pH Fe(II) oxidation at Hughes Borehole, Portage, Pennsylvania. Mine Water Environ. 29, 239–247. http://dx.doi.org/10.1007/s10230-010-0105-5.

Druschel, G., Baker, B., Gihring, T., Banfield, J., 2004. Acid mine drainage biogeochemistry at Iron Mountain, California. Geochem. Trans. 5, 13.

Edwards, K.J., Gihring, T.M., Banfield, J.F., 1999. Seasonal variations in microbial populations and environmental conditions in an extreme acid mine drainage environment. Appl. Environ. Microbiol. 65, 3627–3632.

Gammons, C.H., Duaime, T.E., Parker, S.R., Poulson, S.R., Kennelly, P., 2010. Geochemistry and stable isotope investigation of acid mine drainage associated with abandoned coal mines in central Montana, USA. Chem. Geol. 269, 100–112. http://dx.doi.org/10.1016/j.chemgeo.2009.05.026.

Gammons, C.H., Nimick, D.A., Parker, S.R., Snyder, D.M., McCleskey, R.B., Amils, R., Poulson, S.R., 2008. Photoreduction fuels biogeochemical cycling of iron in Spain's acid rivers. Chem. Geol. 252, 202–213. http://dx.doi.org/10.1016/j.chemgeo.2008.03.004.

Hallberg, K.B., 2010. New perspectives in acid mine drainage microbiology. Hydrometallurgy 104, 448–453. http://dx.doi.org/10.1016/j.hydromet.2009.12.013.

Hedin, R.S., Nairn, R.W., 1992. Designing and sizing passive mine drainage treatment systems., 13th Annual WV Surface Mine Drainage Task Force Symposium. http://wvmdtaskforce.com/proceedings/1992.cfm.

Hedrich, S., Schlömann, M., Johnson, D.B., 2011. The iron-oxidizing proteobacteria. Microbiology 157, 1551–1564. http://dx.doi.org/10.1099/mic.0.045344-0.

Kirby, C.S., Elder-Brady, J.A., 1998. Field determination of Fe^{2+} oxidation rates in acid mine drainage using a continuously-stirred tank reactor. Appl. Geochem. 13, 509–520. http://dx.doi.org/10.1016/S0883-2927(97)00077-2.

Kirby, C.S., Cravotta, C.A., 2005. Net alkalinity and net acidity 1: theoretical considerations. Appl. Geochem. 20, 1920–1940. http://dx.doi.org/10.1016/j.apgeochem.2005.07.002.

Kirby, C.S., Thomas, H.M., Southam, G., Donald, R., 1999. Relative contributions of abiotic and biological factors in Fe(II) oxidation in mine drainage. Appl. Geochem. 14, 511–530. http://dx.doi.org/10.1016/s0883-2927(98)00071-7.

Leistel, J.M., Marcoux, E., Thiéblemont, D., Quesada, C., Sánchez, A., Almodóvar, G.R., Pascual, E., Sáez, R., 1997. The volcanic-hosted massive sulphide deposits of the Iberian Pyrite Belt Review and preface to the Thematic Issue. Miner. Deposi. 33, 2–30. http://dx.doi.org/10.1007/s001260050130.

Meruane, G., Vargas, T., 2003. Bacterial oxidation of ferrous iron by Acidithiobacillus ferrooxidans in the pH range 2.5–7.0. Hydrometallurgy 71, 149–158. http://dx.doi.org/10.1016/s0304-386x(03)00151-8.

Nagpal, S., 1997. A structured model for Thiobacillus ferrooxidans growth on ferrous iron. Biotechnol. Bioeng. 53, 310–319. http://dx.doi.org/10.1002/(sici)1097-0290(19970205)53:3<310::aid-bit10>3.0.co;2-o.

Nordstrom, D., 1985. The rate of ferrous iron oxidation in a stream receiving acid mine effluent. Selected papers in the hydrologic sciences: U.S. Geological Survey Water-Supply Paper 2270, p. 113-119.

Nordstrom, D.K., 2011. Hydrogeochemical processes governing the origin, transport and fate of major and trace elements from mine wastes and mineralized rock to surface waters. Appl. Geochem. 26, 1777–1791. http://dx.doi.org/10.1016/j.apgeochem.2011.06.002.

Nordstrom, D.K., Alpers, C.N., Ptacek, C.J., Blowes, D.W., 1999. Negative pH and extremely acidic mine waters from iron mountain, California. Environ. Sci. Technol. 34, 254–258. http://dx.doi.org/10.1021/es990646v.

Olem, H., Unz, R.F., 1977. Acid mine drainage treatment with rotating biological contactors. Biotechnol. Bioeng. 19, 1475–1491. http://dx.doi.org/10.1002/bit.260191006.

Pellicori, D.A., Gammons, C.H., Poulson, S.R., 2005. Geochemistry and stable isotope composition of the Berkeley pit lake and surrounding mine waters, Butte, Montana. Appl. Geochem. 20, 2116–2137. http://dx.doi.org/10.1016/j.apgeochem.2005.07.010.

Pennsylvania Department of Environmental Protection (DEP), 2010. 2010 Pennsylvania Integrated Water Qualiy Monitoring and Assessment Report; Clean Water Act, Section 305(b) Report and 303(d) List. Report, In Protection, D.o.E. (Ed).

Pesic, B., Oliver, D.J., Wichlacz, P., 1989. An electrochemical method of measuring the oxidation rate of ferrous to ferric iron with oxygen in the presence of Thiobacillus ferrooxidans. Biotechnol. Bioeng. 33, 428–439. http://dx.doi.org/10.1002/bit.260330408.

Price, W.A., 2003. Challenges posed by metal leaching and acid rock drainage, and approaches used to address them. In: Jambor, J.L., Blowes, D.W., Ritchie, A.I.M. (Eds.), Environmental Aspects of Mine wastes. In: Short Course Series, 31. Mineralogical Association of Canada, Vancouver, pp. 1–10.

Regenspurg, S., Brand, A., Peiffer, S., 2004. Formation and stability of schwertmannite in acidic mining lakes. Geochim. Cosmochim. Acta 68, 1185–1197. http://dx.doi.org/10.1016/j.gca.2003.07.015.

Sánchez España, J., López Pamo, E., Santofimia, E., Aduvire, O., Reyes, J., Barettino, D., 2005. Acid mine drainage in the Iberian Pyrite Belt (Odiel river watershed, Huelva, SW Spain): geochemistry, mineralogy and environmental implications. Appl. Geochem. 20, 1320–1356. http://dx.doi.org/10.1016/j.apgeochem.2005.01.011.

Sánchez España, J., López Pamo, E., Santofimia Pastor, E., 2007a. The oxidation of ferrous iron in acidic mine effluents from the Iberian Pyrite Belt (Odiel Basin, Huelva, Spain): field and laboratory rates. J. Geochem. Explor. 92, 120–132. http://dx.doi.org/10.1016/j.gexplo.2006.08.010.

Sánchez España, J., Santofimia Pastor, E., López Pamo, E., 2007b. Iron terraces in acid mine drainage systems: a discussion about the organic and inorganic factors involved in their formation through observations from the Tintillo acidic river (Riotinto mine, Huelva, Spain). Geosphere 3, 133–151. http://dx.doi.org/10.1130/ges00069.1.

Seal, R.R., Kiah, G.R., Nadine, M.P., Besser, J.M., Coles, J.F., Hammarstrom, J.M., 2010. Aquatic Assessment of the Ely Copper Mine Superfund Site, Vershire Vermont. US Geological Survey, Scientific Investigations Report 2010–5084.

Stookey, L.L., 1970. Ferrozine––a new spectrophotometric reagent for iron. Anal. Chem. 42, 779–781. http://dx.doi.org/10.1021/ac60289a016.

Stumm, W., Morgan, J.J., 1996. Aquatic Chemistry: Chemical Equilibria and Rates in Natural Waters, third ed. John Wiley & Sons, New York.

Tarutis Jr, W.J., Stark, L.R., Williams, F.M., 1999. Sizing and performance estimation of coal mine drainage wetlands. Ecol. Eng. 12, 353–372. http://dx.doi.org/10.1016/s0925-8574(98)00114-1.

Trout Unlimited, 2011. The West Branch Susquehanna Recovery Benchmark Project. Trout Unlimited Eastern Abandoned Mine Program, Lock Haven, PA.

Watzlaf, G.R., Schroeder, K.T., Kleinmann, R.L.P., Kairies, C.L., Nairn, R.W., 2002. The Passive Treatment of Coal Mine Drainage. American Society of Mining and Reclamation, Lexington, Kentucky.

Webster, J.G., Swedlund, P.J., Webster, K.S., 1998. Trace metal adsorption onto an acid mine drainage iron(III) oxy hydroxy sulfate. Environ. Sci. Technol. 32 (10), 1361–1368.

White, D.C., Davis, W.M., Nickels, J.S., King, J.D., Bobbie, R.J., 1979. Determination of the sedimentary microbial biomass by extractible lipid phosphate. Oecologia 40, 51–62. http://dx.doi.org/10.1007/bf00388810.

Williamson, M.A., Kirby, C.S., Rimstidt, J.D., 2006. Iron dynamics in acid mine drainage. In: 7th Internat. Conf. Acid Rock Drainage. American Society of Mining and Reclamation, St. Louis, MO, pp. 2411–2423.

Yu, J.-Y., Heo, B., Choi, I.-K., Cho, J.-P., Chang, H.-W., 1999. Apparent solubilities of schwertmannite and ferrihydrite in natural stream waters polluted by mine drainage. Geochim. Cosmochim. Acta 63, 3407–3416. http://dx.doi.org/10.1016/s0016-7037(99)00261-6.

Ziemkiewicz, P.F., Skousen, J.G., Brant, D.L., Sterner, P.L., Lovett, R.J., 1997. Acid mine drainage treatment with armored limestone in open limestone channels. J. Environ. Qual. 26, 1017–1024. http://dx.doi.org/10.2134/jeq1997.00472425002600040013x.